QUANTIFICATION OF THE STATES AND REACTIVITY OF ZIRCONIUM-BASED METAL-ORGANIC FRAMEWORK SURFACES WITH ORGANOSILANES

WPI

Abigail D. Berube
In partial requirements for the
Degree of Bachelor of Science, B.S. in Chemistry
submitted to the Faculty of

WORCESTER POLYTECHNIC INSTITUTE
100 Institute Road
Worcester, Massachusetts 01609

CONTENTS

LIST OF FIGURES

LIST OF TABLES

PREFACE

A zirconium-based metal-organic framework (MOF), UiO–66, was synthesized to further understand the reactivity of its surface. Motivated by previous MOF research, we are interested in learning more about the role MOF's porous structure can play in controlled trap and release for future therapeutic drug delivery. We hypothesized that organosilanes would have strong covalent monolayer attachment to the surface of UiO–66. Synthesized and silane-derivitized UiO–66 crystals went through a series of experiments to understand the interactions between the silanes and UiO surface. Powder X-ray diffraction (pXRD) supported UiO synthesis, while X-ray photoelectron spectroscopy (XPS) characterized the surface. *In vacuo* Ar^+ sputtering and temperature-programmed desorption (TPD) evaluated surface bonding strengths. Both a theoretical substrate-overlayer and first order desorption model was employed to interpret results. We have shown that a monolayer of silanes will covalently attach to the surface of UiO–66 giving more insight into the UiO family.

ACKNOWLEDGMENTS

I would first like to thank Professor Shawn Burdette and his lab for their support and assistance as well as the space for the UiO–66 synthesis, and Erin Hickey for so kindly answering my many questions. Thank you to everyone in the Grimmgroup who has assisted and supported me during this project and making every day in lab even more enjoyable. I would also like to thank Julia Martin for fielding my seemingly endless questions as I would not be where I am without your guidance in the lab. This project would not have been possible without the groundwork put forth by Becca Dawley and the substantial additions made by Nate Keyes, I thank you both for that and everything you taught me in our time together. I would especially like to thank Professor Ron Grimm for not only advising this project, but for being a mentor for me during my time at WPI. I am forever grateful for all of the advice and encouragement you have given me both in and out of lab and I would not be where I am today without it.

Additionally, I would like to extend a special thank you to David LePré for financially supporting this project during the summer and allowing me to further my skills within the lab.

A. D. B.

GLOSSARY

BDC	1,4-benzenedicarboxylic acid (shown) or 1,4-benzenedicarboxylate 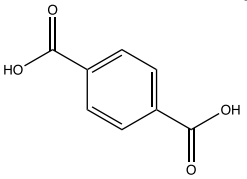
DCM	Dichloromethane
DEF	*N*,*N*-diethylformamide 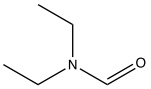
FAT	Fixed-analyzer transmission (mode)
fwhm	Full-width at half-maximum
HDPE	High-density polyethylene

IMFP	Inelastic mean free path
IPA	Isopropanol
MOF	Metal-organic framework
PTFE	Poly(tetrafluoroethylene), *a.k.a.* Teflon
pXRD	Powder X-ray diffraction
TPD	Temperature-programmed desorption
TGA	Thermogravimetric analysis
UHV	Ultrahigh vacuum
XPS	X-ray Photoelectron Spectra/Spectroscopy

SYMBOLS

	Photoelectron terms:
$a_{\mathrm{UiO–66}}$	UiO–66 cubic unit cell length
$\langle A \rangle$	Average atomic mass
d	Depth or distance into material
$D\,(E_{\mathrm{A}})$	Detector efficiency at energy E of A*th* overlayer component
E	Photoelectron kinetic energy
I	Photoelectron intensity
I_0	X-ray flux
h	Planck's constant
N_{A}	Volumetric number density of A*th* overlayer component
SF	Sensitivity Factor
$T\,(E_{\mathrm{A}})$	Analyzer transmission function at energy E of A*th* overlayer component

$\langle Z \rangle$	Average atomic number
Φ	Fractional (surface) coverage
λ	Attenuation length
ν	Frequency of light
ρ	Density
σ_{A}	Surface number density of A*th* overlayer component
θ	Angle of detector collection with respect to surface normal

Thermal desorption terms:

A	Arrhenius preexponential factor
E_{a}	Arrhenius activation energy
n	Order of thermal desorption
R	Gas constant
T	Temperature
β	Heating rate

CHAPTER 1

INTRODUCTION

Metal-Organic Frameworks (MOFs) are a highly customizable group of nanocontainer materials that are valued for their porosity. Typically, these structures consist of metal-oxygen clusters that are bridged together by a long organic linker that gives them their porous structure.[1] Due to this cluster-linker structure, interchanging different metal clusters and organic linkers yields a wide range of MOF structures with tunable pore sizes and chemistries for different applications.[1] This tunability has led to the discovery and studies of more than twenty thousand unique MOF structures over the last decade, and investigation into different applications.[2] Some of these applications include but are not limited to catalysis, molecular storage, and separation.[2]

Among the applications being investigated, what brought MOFs to our attention was their capability for possible trap and release of molecular guests within their porous structure. To be able to have trap and release, you must have control of the guest release in some capacity. Different types of trap and release control with MOFs have been investigated including pressure-based load and release, thermal breakdown of the MOF for release,[3] or surface modification to seal the pores.[4] Surface modification for different applications has

previously been investigated, but until recently has not been used to seal guests into the pores of the MOF.[4] This has been denoted as capping the MOF. Surface attachment is done without changing any internal structure or chemistry of the MOF.[5] This is important for preserving the MOF's already highly stable structure to allow for the most efficiently controlled trap and release of a guest molecule from within its pores.

Attempts at guest trapping and capping within a MOF have been done previously in our group using a zinc-based MOF, MOF–5. One attempt at trap and release with MOF–5 was done by the sorption of a guest inside the pores, attaching a sterically hindering cap to the surface of MOF–5, and then submerging the capped MOF in ethanol to watch the release of dye through the caps over a period of time.[5] A second study showed control over the release of guests from MOF–5 pores through photolysis of the capping molecules to have on demand release of guests. The molecules attached to the surface was sterically bulky enough to seal the dye into the pores and was able to be degraded through photolysis.[4] As shown, the ability to have controlled trap and release of molecular guests using a MOF structure, makes them great contenders to play a role in drug delivery.

Zirconium terephthalate MOF UiO–66 may be an alternative to MOF–5 for surface attachment studies. UiO–66 is comprised of zirconium-oxygen based clusters with strong coordination bonds to 1,4-benzenedicarboxylate (BDC) linkers to form a framework with high connectivity.[6,7] Due to its high thermal and chemical stability, it has become one of the more promising MOF materials. Having stability in air and water is crucial for its biocompatibility and for research in drug delivery.[6,7] Aside from its structural stability, understanding what is happening on the surface is imperative for understanding its trap and release ability. Rebecca A. Dawley from our group previously inferred that the bonding of twelve BDC molecules via carbonate groups with a –1 charge implies a charge of +12 on each inorganic cluster. For a +12 charge, six Zr^{4+} are well balanced by four O^{2-} and four $(OH)^{1-}$ species. Due to this, she was able to hypothesize that the purely basic Zr–OH moieties should be reactive towards acidic silanes that form monolayers on metal oxide surfaces at hydroxyl sites, and thus should produce the same on the surface of UiO–66.[8] With this assumption, she initiated trials of attaching fluorinated silane molecules to the surface of UiO–66. These attempts did confirm attachment, but overshot the target of a single monolayer on the surface due to possibly bad reactant.[8] Reaching a monolayer of surface attachment to the surface of UiO–66 motivates our present study.

Herein, we synthesized single-crystal UiO–66 to understand the connectivity and stability of a monolayer of covalently bonded silane-based capping molecules to the surface of UiO–66. Powder X-ray diffraction (pXRD) supported the crystalline synthesis of UiO–66. X-ray photoelectron spectroscopy (XPS) characterized UiO–66 prior to and after exposure to trichloro- and

triethoxy- organosilanes. We utilized trifluoropropyl as the organic group for the high sensitivity of XPS towards fluorine atoms, and for the absence of adventitious fluorine signals that otherwise complicate the interpretation of oxygen and carbon regions. Argon-ion sputtering results probed the surface attachment of the capping silane molecules to UiO–66. Temperature-programed desorption (TPD) further characterized the bond strengths of UiO–66 to the silane molecules. The result of this study brings new light to the capabilities of the UiO MOF family for trapping and capping and future therapeutic drug delivery.

CHAPTER 2

EXPERIMENTAL SECTION

2.1 Materials and Chemicals

All chemicals were used as received unless otherwise noted. Chemicals used in synthesizing metal organic framework UiO–66 included zirconium dichloride oxide hydrate ($ZrOCl_2 \cdot x\,H_2O$, 99.9% metal basis, Alfa Aesar), terephthalic acid (BDC, 99+%, Acros Organics), formic acid (97%, Alfa Aesar), and N,N-diethylformamide (DEF, >99.0% Tokyo Chemical Industry). The DEF was dried through a vacuum distillation onto activated molecular sieves (3Å, 1–2 mm beads, Alfa Aesar). Silane capping utilized both trichloro-based and trialkoxy-based silane solutions. Toluene (≥99.5%, Fisher Chemical) from a commercial solvent system (Phoenix SDS, JC Meyer Solvent Systems, Irvine, California) was stored over activated sieves and placed under argon on a Schlenk line for air-free use. Silanes included (3,3,3-trifluoropropyl)trichlorosilane (97%, Alfa Aesar), (3,3,3-trifluoropropyl)trimethoxysilane (>98.0%,Tokyo Chemical Industry) and (4-chlorophenyl)trimethoxysilane (97%, Aldrich). Toluene diluted the (3,3,3-trifluoropropyl)trichlorosilane to ~100 μM before use. Trialkoxy silane solutions were created

when needed inside of the flush box in an air free environment (Polypropylene Twin Glovebox, Terra Universal, Fullerton, California) with dry toluene. Ethanol (200 proof, absolute, anhydrous, Pharmco) diluted acetic acid (glacial, Fisher Chemical) for use with silanes.

Other chemicals used included isopropanol (IPA, 99.6%, Acros Organics), sulfuric acid (95–98%, Sigma-Aldrich) and hydrogen peroxide (30% in water, Fisher Bioreagents) for piranha solution, and dichloromethane (DCM, 99.5%, VWR Chemicals BDH). Argon gas (ultrahigh purity, UHP, Airgas) was used for drying.

2.2 Crystal Synthesis

UiO–66 was synthesized with a procedure fine-tuned by Boisonnault and co-workers,[9] Trickett and co-workers,[10] and Rebecca A. Dawley[8] from our laboratory.

Before starting any synthesis, the oven (Yamato constant temperature drying oven DVS402) was set to a built-in auto-stop program for 173 °C, which is read from an internal thermocouple at 135 °C. Different tests proved that the programmed temperature and the actual internal temperature were constantly 30–40 ° off.[8] This program runs for 48 hours at that temperature. Meanwhile, as the oven heats up, opened and marked vials specific to the current trial and their lids along with a spatula were pumped into a recirculating glove box. Recirculating nitrogen-purged glove box had an active catalyst and a box O_2 pressure of <2 ppm. Once in the chamber, the items went through three 5-min pump cycles to ensure no moisture was brought in. It was found that a range of 12–15 mg of $ZrOCl_2$ could be used. Vials for each respective trial were filled with a consistent amount of $ZrOCl_2$ and capped. Once removed from the glovebox, 4 mL of dried DEF dissolved the metal salt and was then sonicated for ~30 s. Around 5 mg of the linker BDC was added to each vial, along with 4 mL of formic acid. The vials were then capped and set into the now heated oven for the allotted 48 hours. Once finished, they were left as is until time of use.

2.3 Silicon silanization trials

Proof of concept trials of silane attachment on silicon wafer surfaces were done for two different silanes. Trials were based on procedures from Glass and collaborators[11] and Waddell and collaborators.[12] Piranha solution was made in a 3:1 ratio of hydrogen peroxide to sulfuric acid. Trials denoted with ADBNDK were done in collaboration with Nathaniel D. Keyes from our group. The first trial was done with (3,3,3-trifluroropropyl)trichlorosilane, as show in line one of Table 2.1. The wafers were piranha etched and then

Table 2.1: **Names, types of silanes, and concentrations of different silicon silanization trials.**

Trial Name	Silane	Conc. (mM)
001ADBNDK	(3,3,3,-trifluroropropyl)trichlorosilane	0.10
001ADBRRR	(4-chlorophenyl)triethoxysilane	38.9
002ADBRRR	(4-chlorophenyl)triethoxysilane	77.8
003ADBRRR	(4-chlorophenyl)triethoxysilane	156

exposed to 4 mL of the silane solution in microcentrifuge tubes. Three exposures were done, one for 2 minutes, one for 10 minutes, and one for 100 minutes. They were washed once with 2 mL of toluene and twice with 2 mL of DCM.

Trials denoted with ADBRRR were done in collaboration with Rebecca R. Ramthun from our group. 001ADBRRR was done on a freshly piranha solution-cleaned silicon wafer. The wafer sat in solution for ~3 min and then thoroughly cleaned with water. Inside of a vial, the wafer was added with a drop of water, capped, and then pumped into the recirculating flush box. Once inside, 1 mL of the silane solution was added to the vial, capped again, and exposed for 1 hour. After, the vial was removed from the flush box and the silane solution was decanted off. Then, 1–2 mL of dry toluene was added for washing and decanted off. This was done two more times with ethanol, and the wafer was stored in ethanol until use.

Trial 002ADBRRR was done on a silicon wafer that had been piranha cleaned for 15 minutes. Once added to a vial, the wafer was pumped into the flush box and 5 mL of the silane solution was added. The wafer was exposed to the silane solution for ~18 hours. After, the vial was brought out of the flush box and the silane was decanted. 5 mL of dry toluene was added and then the wafer was sonicated for 5 min. Toluene was decanted, and two similar washes with ethanol followed with no sonication. The wafer was stored in ethanol until future use.

Trial 003ADBRRR was done on a silicon wafer from the same batch as trial 002ADBRR. Once added to the vial, the wafer was pumped into the flush box and 200 μL of silane was added. The vial was removed from the flush box and 5 mL of undried-bottle toluene was added. The wafer was exposed to the silane solution for 4 hours, in a 60 °C oil bath with 500 rpm of stirring and a parafilm lid. After, the silane was decanted, 5 mL of dry toluene was added and then the wafer was sonicated for 5 min. Toluene was decanted, and two similar washes with ethanol followed with no sonication. The wafer was stored in ethanol until future use.

2.4 Capping Trials

The results from 001ADBNDK trial in Table 1 were used as guidelines for capping UiO–66 crystals with the (3,3,3-trifluoropropyl)trichlorosilane. Both volume of silane solution used, and time were varied until the XP spectra indicated a monolayer-adjacent of silane on the surface of the MOF. Exposures during these trials varied from 10 minutes to 20 hours, with from 2 mL to 4 mL of silane included. This ended up being 4 mL of silane solution and 20 hours of exposure to establish a relationship of fluorine-to-zirconium ratios in the XP spectra that were representative of a monolayer attachment. From here, a general capping procedure was deduced.

UiO–66 crystal vials were cracked open with locking pliers and were entirely decanted into a 15 mL plastic centrifuge tube. Water was used in a second centrifuge tube as a counterbalance for use of the centrifuge. Each UiO–66 crystal solution was spun at 3900 rpm for 2 min and remaining DEF and formic acid solution was decanted into waste with a plastic pipette. No more than 5 mL of any silane solution was added into the centrifuge tube along with a stir bar. The solution was then left stirring overnight to ensure silane attachment to the MOF. The solutions were again spun down in a centrifuge, this time with the silane solution decanted from the crystals. Toluene was then added and sonicated for 30 seconds and decanted off. Depending on the silane, two more washes were done with either ethanol or DCM. Crystals were then ready to be characterized to determine cap attachment.

The procedure for (3,3,3-trifluoropropyl)trimethoxysilane was based on trials 001-003ADBRRR with an addition of 1 mL of 0.1% acetic acid in ethanol during silane exposure.

2.5 Sample Preparation for Ultrahigh Vacuum Experiments

A few milligrams of a suspension of capped crystals were pipetted onto the center of an IPA prepped XPS puck. If there was still some rinse solvent in the sample, no carbon tape was needed. The puck was then carefully placed into a Schlenk drying chamber and pumped on a Schlenk line for a minimum of five hours, but typically overnight. For this, an argon-purged Schlenk line with an oil diffusion pump was used with a base pressure of less than 1×10^{-3} torr. Once the sample was dried, it was transferred into the load lock of the XPS chamber and allowed to be pumped down to ultrahigh vacuum (UHV) levels. Once fully pumped down, the puck could be transferred into the main chamber for scanning or sputtering.

Samples that were intended for TPD were prepped the same way but instead on a TPD-specific puck. A larger puck that allowed for higher temperature ramping due to its ceramic core.

2.6 pXRD Sample Prep

To confirm the XRD trace of a sample of UiO–66, a PTFE (Teflon) XRD sample plate was used. UiO–66 synthesis produces a tiny amount of crystal product, so the back side of the sample holder was used. Slightly solvated crystal was used to ensure the sample stuck during scans.

2.7 X-ray Photoelectron Spectroscopy

All X-ray photoelectron (XP) spectra was acquired by a PHI 5600 XPS system with a third-party data acquisition system (RBD Instruments, Bend Oregon) as used in previous publications.[13] The base pressures of the main analysis chamber were below 1×10^{-9} torr. Monochromated Al Kα X-rays were produced at a 90° angle with respect to the takeoff angle for the hemispherical energy analyzer and in all studies a level sample puck with a normal angle that bisected the incoming X-rays and detected electrons. Wide-energy survey scans utilized a 117-eV pass energy, 0.5 eV step size, and 50 ms per step. High-resolution scans of the C 1s, F 1s, O 1s, Zr 3d, Si 2p, and Cl 2p regions employed a 23.5 eV pass energy, 0.025 eV step size, and 50 ms per step. All UiO–66 crystal samples required charge neutralization. Neutralization parameters were optimized to yield a C 1s with the narrowest possible fwhm feature that remained between 286–281 eV that was linearly shifted to 285.0 eV following data acquisition.

Peak fitting utilized a LabVIEW-based program fabricated in house based on literature for spectral shapes corrected for sensitivity factors for the specific instrument,[14,15] and background-energy-loss functions.[16–18] Each peak shape is described by a pseudo-Voight-style function, GL(x), where x scales nonlinearly from pure Gaussian ($x = 0$) to a pure Lorentzian ($x = 100$) shape. Fitting of the C 1s and Zr 3d peaks from frame A of Fig. 4.2 employ a Tougaard style background, and the O 1s region employs a linear background. Fitting of the C 1s, O 1s, and Zr 3d5 peaks from frame B of Fig. 4.2 employ a Tougaard style background, and F 1s, Si 2p, and Cl 2p employ a linear background. Fitting of the C 1s and O 1s peaks from frame C of Fig. 4.2 employ a Tougaard style background, the Zr 3d, F 1s, and Cl 2p regions employ a Shirley style background, and the Si 2p region employs a linear background. Fitting of the C 1s, O 1s, Zr 3d, and F 1s regions from Fig. 4.3 employ a Tougaard style background, and Si 2p region employs a linear fit.

2.8 Temperature-Programmed Desorption

TPD experiments were conducted inside of an in-house-modified chamber attached to the PHI5600 analysis chamber which is turbopumped separately and isolated from the XPS as needed, as described in previous publications.[19]

A custom-fabricated molybdenum sample puck with a ceramic resistive heating core that mimics the shape of the Phi sample puck was utilized for all TPD experiments (HeatWave Labs, Inc., Watsonville, CA). The sample puck was fitting with tungsten wire prongs for thermocouple connection. The chamber is equipped with a removable port sealed with a Viton gasket for sample introduction, as well as a transfer arm that allows for sample passage from the TPD chamber to the XPS main chamber. For the mass spectrometer, a 1–200 amu quadrupole mass selector with a channel-electron multiplier (channeltron) and a 70-eV, electron-impact ionization source (RGA200, Stanford Research Systems, Sunnyvale CS) is affixed to the top of the chamber. Within the chamber, there is a stage that can raise and lower the sample puck within 5 mm of the mass spectrometer entrance grid. Sample heating came from current passing through electrical connections on the sample stage to connection on the custom sample puck. Data acquisition came from an in-house designed LabVIEW-based program which controlled the power supply (PGM-2010, GW Instek, New Taipei City, Taiwan) while simultaneously collecting mass spectra as a function of time. During heating of (3,3,3-trifluoropropyl)trichlorosilane-derivatized UiO–66, the mass spectrometer quantified the intensities of species desorbing from the surface at 31 m/z and 97 m/z.

CHAPTER 3

THEORETICAL SECTION

3.1 Overlayer Model for Interpretation of X-ray Photoelectron Spectra

3.1.1 Description of the Overlayer Model

The quantification of the silane-derivatized UiO–66 surface employs a substrate-overlayer model to connect experimental photoelectron peak-area ratios with possible coverage models for silanes on a MOF surface. That is to say, the intention is to describe the experimental ratio between the F 1s peak area and the Zr 3d peak area in terms of a physical model for silane adsorption to UiO–66, or $I_{\mathrm{F\ 1s}}$ / $I_{\mathrm{Zr\ 3d}}$. The model employed in this work is based on a model fabricated by Alexander D. Carl and used previously in our group[20–22] which was based on work put forth by Seah and Briggs,[23] Ebel,[24] Fadley,[25,26] and Stranger et al.[27] The relationship of the attenuation of photoelectrons emitted from the UiO–66 substrate layer through the substrate-overlayer is established with this model.

Figure 3.1 presents an idealized coverage cartoon as well as a description necessary for overlayer model calculations. In our model, we assume capping

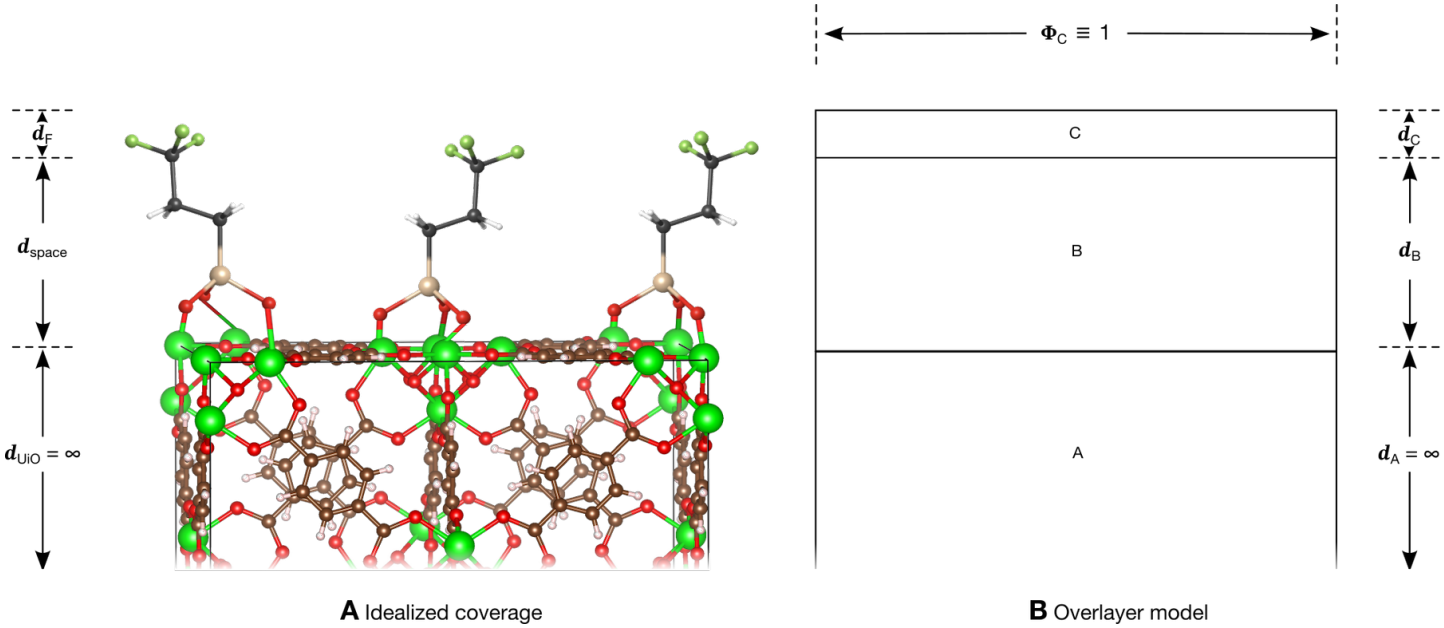

Figure 3.1: Frame A depicts the idealized silane coverage on the surface of UiO–66, frame B depicts the model surface coverage by a uniform monolayer.

on the {100} family of faces on a UiO–66 crystal, and we further assume one silane molecule caps each inorganic cluster. Such an approximation yields a silane coverage of two silanes per 2.07465^2 nm^2 UiO–66 face, or approximately 4.6×10^{13} molecules cm^{-2}. This assumption further yields about a 10× lower coverage than experimentally determined coverages of the similarly sized aminopropylsilane on glass,[28,29] however we believe it is a reasonable starting assumption for coverage calculations. Below, we introduce a generalized three-layer overlayer model before parameterizing it and applying it to a model akin to Figure 3.1A.

Describing the three-layer model requires several variables and equations to be defined. The total photoelectron intensity of a pure, uncovered, and infinitely thick substrate A, denoted as I_A is defined using eq 3.1.

$$I_A = I_0 \, \sigma_A T(E_A) \, D(E_A) \int_0^\infty N_A(z) \exp \frac{-z}{\lambda_{A,self} \cos \theta} dz \tag{3.1}$$

Equation 3.1 includes the density of photons striking the surface area per second, I_0, or X-ray flux. The photoionization cross-section for a specific core-level electron from element A at an energy of $h\nu$, σ_A. The analyzer transmission function, or ratio of electrons of energy E, that enter the lens system and those that ultimately reach the detector is $T(E_A)$ while the detector efficiency for electron of energy E is $D(E_A)$. The number density of atom A within the analyzed material is N_A.

The attenuation length of an electron from material A that is traveling through the pure material A (i.e. travelling through itself), $\lambda_{A,self}$, deserves particular attention. For all XPS data in this study, θ is equal to 45° which is the photoelectron collection angle with respect to the surface normal for typical analyses in our Phi5600 instrument. Beyond escape depths, a determination of overlayer signal intensities fundamentally relies on scattering distances for electrons, or *attenuation lengths*, through a particular material. Closely linked to inelastic mean free path (IMFP) values, attenuation lengths convey what fraction of electrons are not lost and manage to escape while scattering through a solid based on that solid's density of electron scatterers, and the kinetic energy of the photoelectron of interest. Attenuation length values are the subject of significant study for accurate XPS-based quantification of overlayers, and such values are well established for many pure materials and componds.[30–32] However, few reports utilize XPS to quantify relative components or surface coverages of MOF materials, and experimentally determined attenuation lengths may not exist. In contrast to experimental attenuation lengths, heuristic approximations often have limited accuracy but provide attenuation length values with minimal input parameters. Seah and Cumpson derived an empirical model show in eq 3.2 that we have used previously for nontraditional and understudied materials.[33]

$$\lambda = 0.316 \times 10^{12} \left(\frac{\langle A \rangle}{\rho N} \right)^{1/2} \left[\frac{\mathbf{E}}{\langle Z \rangle^{0.45} \left(3 + \ln \frac{\mathbf{E}}{27} \right)} + 4 \right] \tag{3.2}$$

This equation relies on: **E**, the photoelectron kinetic energy; $\langle A \rangle$, the average atomic mass of the species in the overlayer in g mol^{-1}; N, Avogadro's number; ρ, the overlayer density in kg m^{-3}; and the average atomic number for atoms in the overlayer, $\langle Z \rangle$.

Since substrates are typically thicker than both the X-rays can penetrate through and the attenuation length of normal photoelectrons, eq 3.1 can be integrated from the surface, $z = 0$, through ∞. The integration of eq 3.1 yields eq 3.3 which has an unchanging electron escape depth.

$$I_\mathrm{A} = I_0 \, \sigma_\mathrm{A} T(E_\mathrm{A}) \, D(E_\mathrm{A}) \, N_\mathrm{A} \, \lambda_{\mathrm{A,self}} \cos\theta \tag{3.3}$$

However, eq 3.3 would not typically be used alone, as a layered system would have more than one type of intensity to look at. In this case, an intensity ratio would be used. Therefore, the same information must be determined for an element, B, in the overlayer, denoted as I_B. To calculate the intensity of element B in the overlayer 3.4 must be integrated from $z = 0$ to d, a defined depth yielding eq 3.5.

$$I_\mathrm{B} = I_0 \, \sigma_\mathrm{B} T(E_\mathrm{B}) \, D(E_\mathrm{B}) \int_0^d N_\mathrm{B}(z) \exp \frac{-z}{\lambda_{\mathrm{B,self}} \cos\theta} \mathrm{d}z \tag{3.4}$$

$$I_\mathrm{B} = I_0 \, \sigma_\mathrm{B} T(E_\mathrm{B}) \, D(E_\mathrm{B}) \, N_\mathrm{B} \, \lambda_{\mathrm{B,self}} \cos\theta \left(1 - \exp \frac{-d}{\lambda_{\mathrm{B,self}} \cos\theta} \right) \tag{3.5}$$

However, to accurately quantify the fractional coverages or depths of overlayers these equations must be able to be used in tandem. This is given by integrating eq 3.1 from $z = d_\mathrm{B}$ to ∞ to yield eq 3.6, the simplest form of this equation with one uniform overlayer, B.

$$I_\mathrm{A} = I_0 \, \sigma_\mathrm{A} T(E_\mathrm{A}) \, D(E_\mathrm{A}) \, N_\mathrm{A} \, \lambda_{\mathrm{A,self}} \cos\theta \exp \frac{-d_\mathrm{B}}{\lambda_{\mathrm{A,B}} \cos\theta} \tag{3.6}$$

The depth of overlayer B is given by d_B and the attenuation of an electron ejected from substrate A through the overlayer B is given by $\lambda_{\mathrm{A,B}}$. To get the intensity ratio for overlayer B to substrate A, eqs 3.5 and 3.5 are combined and simplified to give eq 3.7.

$$\frac{I_B}{I_A} = \frac{N_B\, SF_B}{N_A\, SF_A} \frac{1 - \exp\frac{-d_B}{\lambda_{B,self}\cos\theta}}{\exp\frac{-d_B}{\lambda_{A,B}\cos\theta}} \tag{3.7}$$

In eq 3.7, energy dependent terms $T(E_A)$ and $D(E_A)$ can be cancelled out for our model because our analyzer is configured to the Fixed Analyzer Transmission mode, FAT, for photoelectron acquisition so all of the electrons are reaching the detector with similar kinetic energies. Since the spectra being acquired is being done at the same time, in the same instrument, under the same θ, the I_0 and initial $\cos\theta$ terms can both be removed. And finally, the σ and λ terms outside of the exponential can be combined into one term, the sensitivity factor, SF. There is a specific value for this for each element being analyzed by the instrument configuration.[14,34]

For an instance in which the coverage is not uniform, $\mathbf{\Phi}_B$ represents fractional coverage of layer B over layer A, while $\mathbf{\Phi}_C$ represents fractional coverage of the whole over layer B such that $\mathbf{\Phi}_C \leq \mathbf{\Phi}_B$. In considering the ratio of a signal from overlayer C relative to a signal from substrate layer A, photoelectrons from layer A under $\mathbf{\Phi}_C$ are attenuated by both layers B and C, or $\mathbf{\Phi}_C \exp\frac{-d_C}{\lambda_{A,C}\cos\theta} \exp\frac{-d_B}{\lambda_{A,B}\cos\theta}$; while photoelectrons under $\mathbf{\Phi}_B$ but not under $\mathbf{\Phi}_C$ are only attenuated by layer B, or $(\mathbf{\Phi}_B - \mathbf{\Phi}_C)\exp\frac{-d_B}{\lambda_{A,B}\cos\theta}$, and the part of A not covered by any other layers are not attenuated at all, or $(1 - \mathbf{\Phi}_B)$. Equation 3.8 represents this generic instance of layers B and C fractionally covering a layer A.

$$\frac{I_C}{I_A} = \frac{N_C\, SF_C}{N_A\, SF_A} \frac{\mathbf{\Phi}_C\left(1 - \exp\frac{-d_C}{\lambda_{C,self}\cos\theta}\right)}{1 - \mathbf{\Phi}_B + \zeta + \xi} \quad \text{...where...} \tag{3.8}$$

$$\zeta \equiv (\mathbf{\Phi}_B - \mathbf{\Phi}_C)\exp\frac{-d_B}{\lambda_{A,B}\cos\theta}$$

$$\xi \equiv \mathbf{\Phi}_C \exp\frac{-d_C}{\lambda_{A,C}\cos\theta}\exp\frac{-d_B}{\lambda_{A,B}\cos\theta}$$

3.1.2 Parameterizing and utilizing the overlayer model

For the application of the generic overlayer model relevant to uniform silane coverage over UiO–66 as in Fig. 3.1, we consider layer C as the fluorine atoms in the $-CF_3$ group on the silane, layer B as the length of the silane space between the fluorine and the UiO–66 surface, and A as the UiO MOF itself. Thus, I_C / I_A represents the target of interest for $I_{F\,1s}$ / $I_{Zr\,3d}$, N_F represents the number density of fluorine atoms in the C layer, N_{Zr} represents the number density of Zr atoms in the A substrate layer, and $SF_{F\,1s}$ and $SF_{Zr\,3d}$ represent the respective sensitivity factors for the C*th* and A*th* layer. Assuming uniform

monolayer coverage of two different overlayers on the substrate leads to significant simplifications where $\mathbf{\Phi}_C = \mathbf{\Phi}_B = 1$. Further, if one assumes that electrons originating in material A undergo similar attenuation when going through both layers B and C, then eq 3.8 simplifies to eq 3.9 where $\lambda_{A,B} = \lambda_{A,C} = \lambda_{A,BC}$. In practice, $\lambda_{C,self}$ represents the attenuation length of F 1s through itself, or $\lambda_{F\,1s,self}$.

$$\frac{I_C}{I_A} = \frac{N_C\, SF_C}{N_A\, SF_A} \frac{1 - \exp \frac{-d_C}{\lambda_{C,self} \cos\theta}}{\exp \frac{-d_B - d_C}{\lambda_{A,BC} \cos\theta}} \tag{3.9}$$

For the model in Fig. 3.1 layer C in frame B represents the fluorine layer in frame A, layer B represents the space between the fluorines and the surface of UiO–66, and layer A represents the UiO–66 unit cell. For this study we treated our attenuation lengths as if the BC layers were similar to that of poly(tetrafluoroethylene), PTFE, yielding eq 3.10.

$$\frac{I_{F\,1s}}{I_{Zr\,3d}} = \frac{N_F\, SF_{F\,1s}}{N_{Zr}\, SF_{Zr\,3d}} \frac{1 - \exp \frac{-d_F}{\lambda_{F\,1s,PTFE} \cos\theta}}{\exp \frac{-d_{space} - d_F}{\lambda_{Zr\,3d,PTFE} \cos\theta}} \tag{3.10}$$

Knowing the depth of the fluorine layer is crucial to calculating the intensity ratios, as well as the number densities for each atom, N_F and N_{Zr}. Importantly, we can simplify the two *volumetric* number density, N, values by considering their related *surface* number density, σ, value because our silane coverage model is considering a particular silane surface packing density *per the surface area of one UiO–66 unit cell face*. Since UiO–66 follows a cubic crystal structure with unit cell dimensions $a_{UiO-66} = b_{UiO-66} = c_{UiO-66} = 2.07465$ nm, the volume of a UiO–66 unit cell is $a^3_{UiO-66} \approx 8.9296$ nm^3. With four inorganic clusters per UiO–66 unit cell volume and six Zr atoms per inorganic cluster, there are twenty four zirconium atoms in a UiO–66 unit cell, or $N_{Zr} \equiv 24\, a^{-3}_{UiO-66}$. Similarly, we defined silane coverage in Fig. 3.1 as two silanes per unit cell face, and three fluorine atoms per silane yields an overall surface silane coverage of $\sigma_F \equiv 6\, a^{-2}_{UiO-66}$. The volumetric number density for fluorine would be related to the surface number density divided by that layer's thickness, or $N_F = \sigma_F / d_F = 6\, a^{-2}_{UiO-66} d_F^{-1}$. Together, the volumetric number density ratio that is represented in eq 3.10 as N_F/N_{Zr} may be simplified $N_F/N_{Zr} = 6\, a_{UiO-66} \,/\, (24\, d_F)$. Updating eq 3.10 with the number density values yields eq 3.11.

$$\frac{I_{F\,1s}}{I_{Zr\,3d}} = \frac{6\, a_{UiO-66}}{24\, d_F} \frac{SF_{F\,1s}}{SF_{Zr\,3d}} \frac{1 - \exp \frac{-d_F}{\lambda_{F\,1s,PTFE} \cos\theta}}{\exp \frac{-d_{space} - d_F}{\lambda_{Zr\,3d,PTFE} \cos\theta}} \tag{3.11}$$

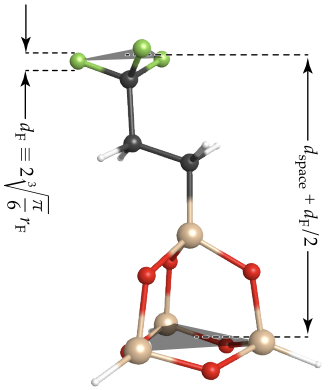

Figure 3.2: AM1 calculation results for silane used with defined distances and thickness employed in the overlayer model.

Assuming the 3,3,3-trifluoropropyl group stands upright and normal to a UiO–66 {100} face, computational chemistry results can approximate spaces can yield d_{space} while fluorine's atomic radius can yield d_F. Frame A in Fig. 3.1 depicts idealized coverage of the silane molecules as well as the defined distances d_F, d_{space}, and d_{UiO} is integrated to ∞. The value for d_{space} was calculated using an AM1-level geometry calculation of the silane molecule attached to a siloxane cluster, depicted in Fig. 3.2. The C–Si bond was oriented to the normal angle of a plane defined by the bottom three tan silicon atoms. The gray triangle connecting those three bottom silicon atoms represent a proxy for the UiO–66 surface itself and the location of interfacial Zr atoms. From the calculation, the distance from the midpoint between the three fluorine atoms with another gray triangle, to the plane defining the proximal UiO–66 surface was $d_{Zr\,to\,F} = 0.698$ nm. A value for d_F was used previously in our group, and was determined by using the length of cubic volume, d_F^3, which is equated to a spherical atomic volume for a given atomic radius, $d_F^3 \equiv 4\pi r_F^3$, therefore $d_F = 2\sqrt[3]{\pi/6}\, r_F$.[20] Using the spherical to equivalent cubic volume calculation for value d is valid because the overlayer model will treat photoelectrons as traveling through uniformly deep layers, so having the layer be represented as hard packed cubes, rather than spheres with free space, is more favorable. Using $r_F = 0.064$ nm from Gray,[35] yields $d_F = 0.103$ nm. Together, Fig. 3.2 demonstrates that we consider $d_{Zr\,to\,F} = d_{space} + d_F/2$, so $d_F/2$ must be subtracted from $d_{Zr\,to\,F}$ yield the organic overlayer depth used for calculations, $d_{space} = 0.647$ nm.

With d values for eq 3.11 established, we next consider attenuation length values, λ, for photogenerated electrons emanating from fluorine atoms and traveling through their own layer, $\lambda_{F\,1s,PTFE}$ as well as electrons emanating from zirconiums atoms in the UiO–66 substrate and being attenuated when

traveling through the silane overlayer, $\lambda_{\mathrm{Zr\,3d,PTFE}}$. We define attenuation value of fluorine photoelectrons traveling through the fluorine layer itself, $\lambda_{\mathrm{F\,1s,PTFE}}$, is defined as 2.05 nm based on work done by Ferraria and collaborators[36] on fluorinated high-density polyethylene (HDPE). For zirconium, we calculate both $\lambda_{\mathrm{Zr\,3d,PTFE}}$ as well as $\lambda_{\mathrm{Zr\,3d,self}}$ although we do not need to use the latter term with our overlayer model.

For Zr 3d photoelectrons traveling through UiO–66, the 180 eV binding energy for Zr 3d yields **E** = 1306.6 eV for 1486.6 eV X-radiation. A UiO–66 unit cell has four $Zr_6O_4(OH)_4$inorganic clusters around which are twelve *p*-benzene dicarboxalate dianions that connect two clusters for a total of 24 BDC dianions per unit cell. Thus, the full stoichiometry of a UiO–66 unit cell is $Zr_{24}O_{128}C_{192}H_{112}$. So a 2.07465^3 nm^3 unit cell yields a density of 880.52 kg m^{-3}, $\langle A\rangle$ = 14.594 g mol^{-1}, and $\langle Z\rangle$ = 406/57 to reveal $\lambda_{\mathrm{Zr\,3d,self}}$ = 4.325 nm.

For Zr 3d photoelectrons traveling through the organic overlayer, **E** remains 1306.6 eV for 1486.6 eV X-rays. An organic layer density of 1500 kg m^{-3} splits the difference between the densities of HDPE and PTFE,[37,38] since we were treating it similarly to PTFE. Further for PDTE, $\langle A\rangle$ = 12.359 g mol^{-1}, and $\langle Z\rangle$ = 6.2143 to reveal $\lambda_{\mathrm{Zr\,3d,PTFE}}$ = 3.233 nm.

Lastly, we employ published sensitivity factors for our Phi5600 with an OmniFocus III lens when collecting photoelectrons at θ = 45° vs the sample surface normal angle, and following excitation with monochromated Al K_α X-radiation that is incident upon the sample at 45° vs the sample surface normal angle and 90° vs the photoelectron takeoff angle. Here $SF_{\mathrm{F\,1s}} \equiv 1$ and $SF_{\mathrm{Zr\,3d}} = 2.216$.[14]

We have defined the remaining terms in eq 3.11 and presented values for the overlayer model for coverage of UiO–66 with two 3,3,3-trifluorosilyl groups per unit cell (one group per inorganic cluster) in eq 3.12.

$$
\begin{aligned}
\frac{I_{\mathrm{F\,1s}}}{I_{\mathrm{Zr\,3d}}} &= \frac{a_{\mathrm{UiO\text{–}66}}}{4\,d_{\mathrm{F}}}\,\frac{SF_{\mathrm{F\,1s}}}{SF_{\mathrm{Zr\,3d}}}\,\frac{1-\exp\frac{-d_{\mathrm{F}}}{\lambda_{\mathrm{F\,1s,PTFE}}\cos\theta}}{\exp\frac{-d_{\mathrm{space}}-d_{\mathrm{F}}}{\lambda_{\mathrm{Zr\,3d,PTFE}}\cos\theta}} \\
&= \frac{2.07465\ \mathrm{nm}}{4\times 0.0103\ \mathrm{nm}}\,\frac{SF_{\mathrm{F\,1s}}}{SF_{\mathrm{Zr\,3d}}}\,\frac{1-\exp\frac{-d_{\mathrm{F}}}{\lambda_{\mathrm{F\,1s,PTFE}}\cos\theta}}{\exp\frac{-d_{\mathrm{space}}-d_{\mathrm{F}}}{\lambda_{\mathrm{Zr\,3d,PTFE}}\cos\theta}} \\
&= \frac{2.07465\ \mathrm{nm}}{4\times 0.0103\ \mathrm{nm}}\,\frac{1}{2.216}\,\frac{1-\exp\frac{-d_{\mathrm{F}}}{\lambda_{\mathrm{F\,1s,PTFE}}\cos\theta}}{\exp\frac{-d_{\mathrm{space}}-d_{\mathrm{F}}}{\lambda_{\mathrm{Zr\,3d,PTFE}}\cos\theta}} \\
&= \frac{2.07465\ \mathrm{nm}}{4\times 0.0103\ \mathrm{nm}}\,\frac{1}{2.216}\,\frac{1-\exp\frac{-0.103\ \mathrm{nm}}{2.05\ \mathrm{nm}\cos 45^\circ}}{\exp\frac{-0.647-0.103\ \mathrm{nm}}{3.233\ \mathrm{nm}\cos 45^\circ}} \\
&= 0.22
\end{aligned}
\tag{3.12}
$$

Thus, we predict a $\frac{I_{F\,1s}}{I_{Zr\,3d}} = 0.22$ for X-ray photoelectron data for an idealized coverage of two fluorinated silanes uniformly attached a UiO–66 surface.

3.2 Models of Thermal Desorption from Surfaces

Data from the TPD experiments were analyzed using the equation for a Redhead-style desorption[39] equation to form a simulated desorption plot, eq 3.13.

$$-\frac{\mathrm{d}N}{\mathrm{d}T} = AN^n\beta^{-1}\exp\frac{-E_\mathrm{a}}{RT} \tag{3.13}$$

Assuming first-order desorption $n = 1$, eq 3.13 uses the sample temperature T, gas constant R, heating rate β, surface density of adsorbed species N, Arrhenius preexponential factor A, and an Arrhenius activation energy, E_a. Due to the first-order assumption, we estimate A as 1×10^{13} s^{-1}.[39] In addition to A, simulated TPD graphs were generated with $N_0 = 1\times10^{12}$, β of 1.5 K s^{-1}, a Δt of 0.1 s starting at 200 °C, and three E_a values of 185, 205, and 225 kJ mol^{-1}. These values were chosen as representative of an ideal desorption of the silane-based molecules from the surface of UiO–66, shown in Fig. 3.1A. Experimentally determined mass vs temperature plots should be comparable to the simulated desorption traces with parametrized E_a values to explore possible values and bounds on realistic E_a values.

The graphs in Fig. 3.3 can be varied to demonstrate that uncertainty in the prexponential factor A yields uncertainties in the determination of E_a with the Redhead model. Increasing A from 1×10^{13} s^{-1} in frame A to 1×10^{16} s^{-1} in frame B while keeping the same E_a values between each frame demonstrates the effect of varying A and proving there is an uncertainty. Comparison of frames A and B in Fig. 3.3 reveals that varying the value of A by three orders of magnitude shifts the entire peak temperature to *lower* temperatures by almost 100 °C. Not only has the peak temperature for the activation energies shifted, but the range of temperature needed to reach the peak has narrowed by nearly 50 °C. If the E_a values were increased, the peaks would shift to the right. This model was also completed with $A = 1\times10^{12}$ s^{-1} and $A = 1\times10^{14}$ s^{-1} which changed the temperature of peak desorption by ±45°C. This demonstrates that we must assume to some degree of uncertainty in ascribing particular E_a while making an a priori assumption of $A = 1\times10^{13}$ s^{-1}.

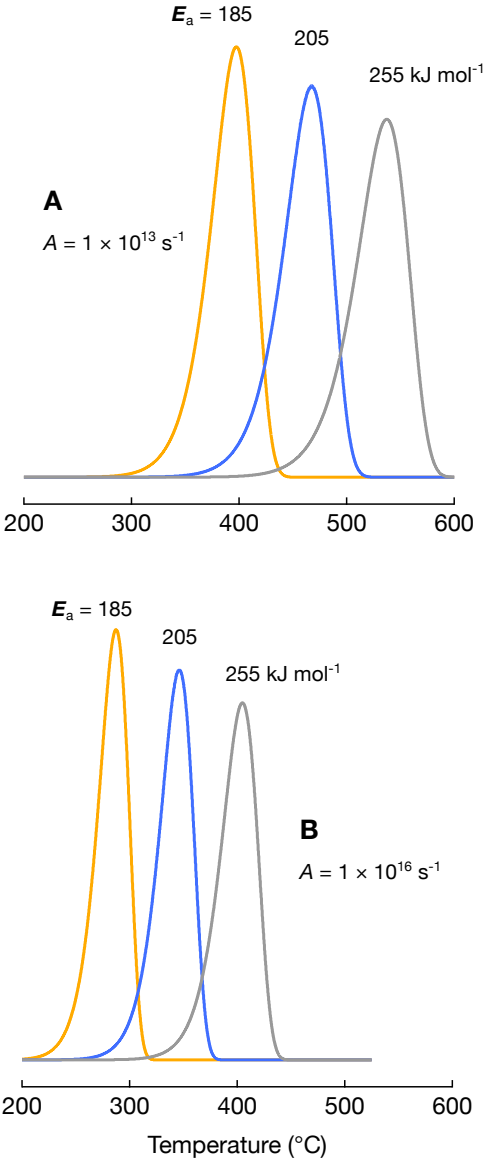

Figure 3.3: Frame A presents modeled first-order desorption fitted with activation energy values of 185 (orange), 205 (blue), and 225 kJ mol^{-1} (gray) and a constant preexponential factor $A = 1 \times 10^{13}$ s^{-1}. Frame B presents the same information, but $A = 1 \times 10^{16}$ s^{-1}.

CHAPTER 4

RESULTS

4.1 Long-Term Stability Studies

Figure 4.1 compares pXRD diffraction traces between a freshly-synthesized UiO–66 sample in frame A, and a sample following storage for fourteen months in the dark under an air ambient in frame B. The trace in Fig. 4.1A was acquired and published previously by Rebecca A. Dawley in our group.[8] The trace of freshly-prepared UiO–66 in Fig. 4.1A demonstrate peaks at 7.38, 8.59, and 12.07°, that respectively indicate reflections from the {111}, {200}, and {220} families of facets. The trace in Fig. 4.1B demonstrates peaks that are well aligned with the three dominant features in Fig. 4.1A, which supports the stability of single crystal UiO–66 following 14 months. The reflection at 2θ = 18° is representative of the PTFE sample holder.[40] From a practical standpoint, this long-term stability enabled the surface science analyses taken in the 2022–2023 academic year presented below that utilized UiO–66 starting material that was synthesized in the summer of 2021.

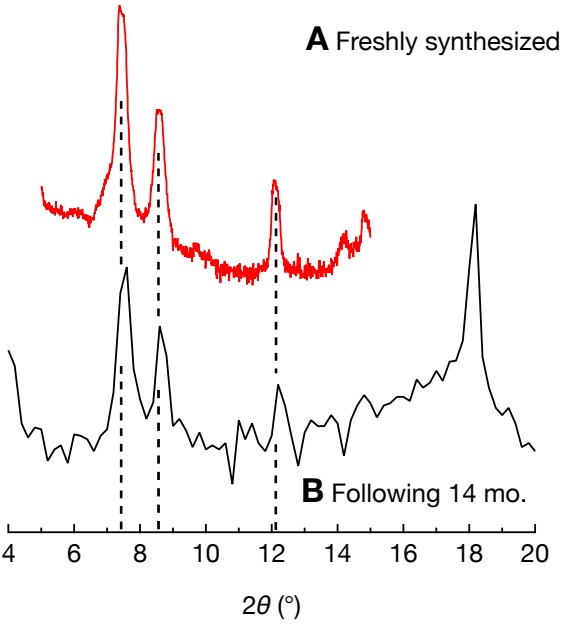

Figure 4.1: Frame A depicts the pXRD trace taken of UiO–66 right after synthesis by Rebecca A. Dawley.[8] Frame B depicts the pXRD trace of UiO–66 14 months after synthesis. Both are on a logarithmic scale.

4.2 Quantification of Silane Attachment and Coverage

Mentioned in Chapter 1, we employed organosilanes with trifluoropropyl organic groups for the high X-ray sensitivity towards fluorine atoms, and the absence of adventitious fluorine signals that can complicate the interpretation of the O 1s and C 1s regions. Further, interpretation of spectral changes due to Ar^+ sputtering further establishes the contribution from near-top-molecular-layer components as may be the case with organosilane adsorption to UiO–66 surfaces.

Figure 4.2 depicts the regions characteristic to both nascent UiO–66 and fluorinated capped UiO–66, F 1s, O 1s, C 1s, Cl 2p, Zr 3d, and Si 2p. Figures C.1, C.2, and C.3 present survey spectra corresponding to the high-resolution spectra in frames A–C. Frame A of Fig 4.2 presents the peaks formed in each region for a nascent sample of UiO–66, and well resembles previously published XP spectra of UiO–66.[41,42] Both Cl 2p and Si 2p are not shown as they are not characteristic for a nascent sample of UiO–66, however a wide-area survey scan as in Fig. C.1 reveals no features ascribable to chlorine or silicon. Throughout Fig. 4.2, The Zr 3d doublet and the O 1s metal oxide feature at 531 eV,[14] are both shaded cyan to highlight their relationship within the UiO–66

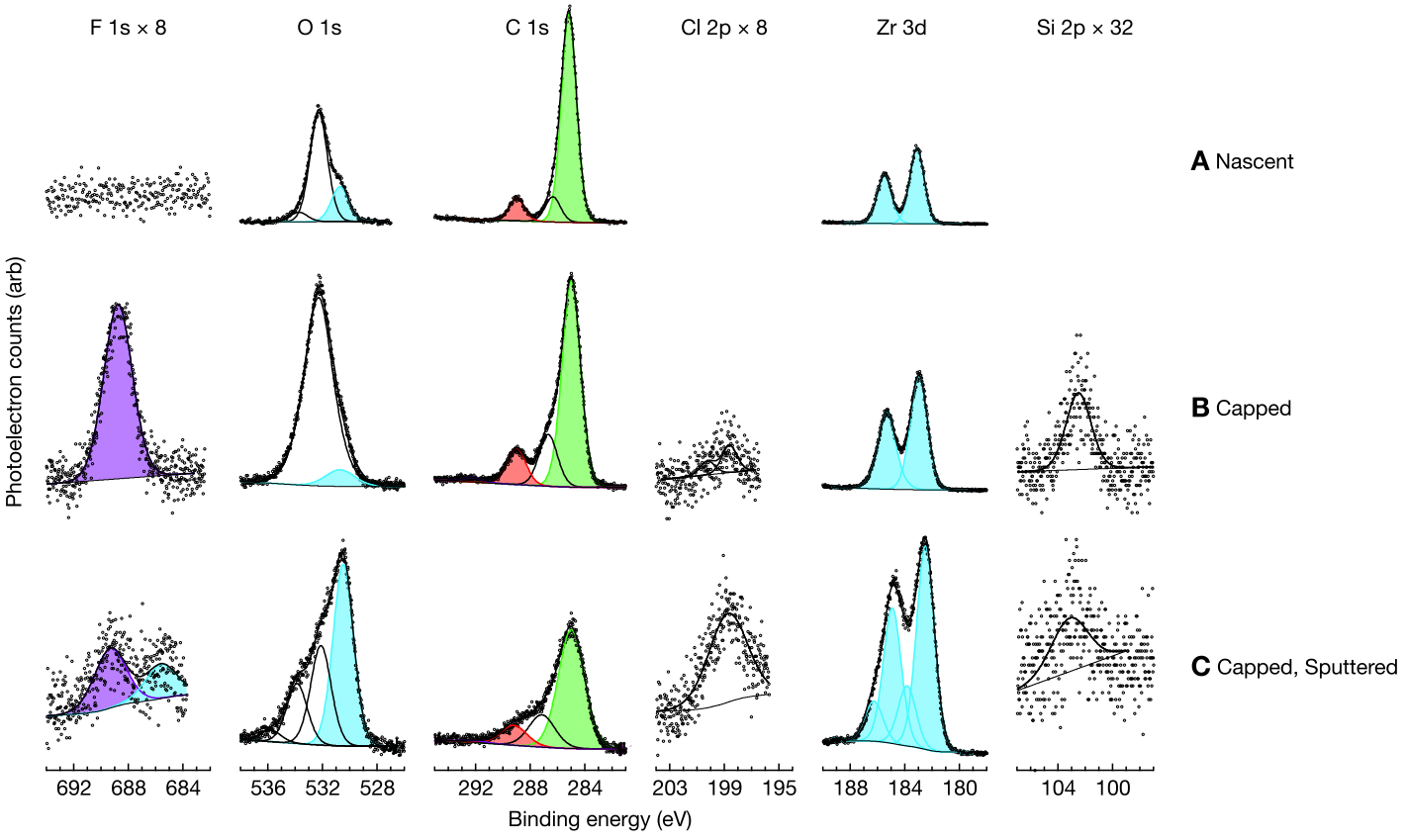

Figure 4.2: XP spectra of UiO–66 (A) as prepared, (B) following a ~20 hr exposure of 100 μM (3,3,3-trifluoropropyl) trichlorosilane, and (C) following 12 s Ar^+ sputtering of a (3,3,3-trifluoropropyl)trichlorosilane-exposed sample. Figures C.1, C.2, and C.3 contain the respective survey spectra.

framework. Within the C 1s region, we ascribe the red-shaded feature at ~289 eV to highly oxidized carbon that is consistent with $-CO_2^-$ acetate groups in the BDC linker.[14] The green-shaded feature at ~285 eV in the C 1s region is consistent with C–C species due to contributions both from the phenyl ring in the BDC linker as well as to adventitious contaminants.[14] Considering a 1:3 ratio of acetate carbon atoms (2) to phenyl carbon atoms (6), each green-shaded feature contains significant adventitious contributions.

Frame B of Fig. 4.2 presents XP spectral regions for UiO–66 following exposure to 100 μM of (3,3,3-trifluoropropyl)trichlorosilane for ~20 hours. Additionally shaded features in Fig. 4.2B include the F 1s feature at 689 eV consistent with organic fluorine as exists for the $–CF_3$ species in the organosilane.[14] We would anticipate a concomitant C 1s feature for the $–CF_3$ carbon in the organosilane, but the ~3.3× lower sensitivity for C 1s vs F 1s and the 3× lower carbon-to-fluorine atom count contributes to a ~10× smaller signal for any $–\mathbf{C}F_3$ carbon vs $–C\mathbf{F}_3$ fluorine. Given the low F 1s signal that are already magnified in Fig. 4.2B, any C 1s feature at 293 eV ascribable to $–CF_3$ is likely below the noise floor in that region.[14] Figure 4.2B demonstrates a small Cl 2p feature whose $2p_{3/2}$ location at 198 eV is characteristic of inorganic chloride. In combination with a F 1s : Cl 2p sensitivity-factor ratio of 1:0.770, the F 1s:Cl 2p peak-area ratio of ~10:1 implies an ~8:1 ratio of detected organic fluorine to inorganic chloride in Fig. 4.2B. A high fluorine-to-chloride ratio that is well above the 1:1 ratio in (3,3,3-trifluoropropyl)trichlorosilane reagent implies significant reactivity of silane attachment and chloride dissociation with UiO–66 exposure. Considering the Cl 2p peak position is consistent with inorganic chloride, we ascribe its presence to reaction byproducts that are trapped in the near-interfacial region of UiO–66 itself. Figure 4.2B also reveals a small Si 2p feature located at 102 eV which is characteristic of silicon in organosilanes. The C 1s:Si 2p sensitivity factor ratio of 0.296:0.283 in combination with the $–CF_3$:Si 2p peak area ratio of ~1.5:1 implies that there is a nearly 1:1 ratio of detected carbon in $–CF_3$ to inorganic silane. The consistency with the 1:1 ratio of C:Si in (3,3,3-trifluoropropyl)trichlorosilane in combination with the lack of Cl 2p intensity, implies significant silane attachment to UiO–66. As expected, an overall lower intensity in the Zr 3d region is depicted in Fig. 4.2B, consistent with a layer of silane attenuating that signal.

While the data in Fig. 4.2B establishes a reaction between the (3,3,3-trifluoropropyl)trichlorosilane and UiO–66, the XP spectra do not a priori confirm surface attachment. To support a model of silane surface attachment, Fig. 4.2C depicts the features of the silanized UiO–66 after 12 s of argon ion sputtering at an acceleration potential of 3.5 kV, an argon source pressure of 25 mPa, and a 5×5 mm^2 source-driven raster. Previous studies in our group established these sputtering conditions removed one monolayer of tantalum oxide every six seconds.[22] Thus, we anticipate that 12 s of argon-ion sputtering removes approximately two monolayers of surface species, and enables sputtering to probe whether silane species are surface localized on

UiO–66. Indeed, the F 1s region contains the most notable change, where the intensity of purple-shaded organic fluorine in Fig. 4.2C is significantly attenuated following sputtering relative to the F 1s area in Fig. 4.2B. The F 1s region in Fig. 4.2C further includes a cyan-shaded contribution at 685~eV that is ascribable metal fluoride species that may be Zr–F that formed due the highly energetic and dissociative sputtering process. Cyan-shaded Zr 3d and metallic O 1s features appear more intense in Fig. 4.2C as we expect based on the removal of surface layers that are otherwise attenuating these signals as in Fig. 4.2B. Similarly, the increase of the Cl 2p feature in Fig. 4.2C compared to Fig. 4.2B may be ascribable to pore-localized but near-surface Cl^- being exposed with the removal of surface species. A model consistent with the totality of results in Fig. 4.2 is a reaction between (3,3,3-trifluoropropyl)trichlorosilane and UiO–66 that results in a surface-localized organosilane species.

Figure 4.2 establishes that the reaction between UiO–66 and (3,3,3-trifluoropropyl)trichlorosilane results in surface-localized organosilane species and can be interpreted in terms of the overlayer model in §3.1.2. An idealized surface coverage of organosilane on the UiO–66 surface in terms of the intensity ratio of F:Zr with an organic layer similar to PTFE is 0.22 or ~1:5. This model can be compared to Fig. 4.2B, where the peak-area ratio of F:Zr is 0.19 or ~1:5, which implies a near-idealized surface coverage of organosilane on UiO–66 when coverage is defined as the attachment of one silane group per inorganic cluster.

Figure 4.3 depicts the XP spectra of UiO–66 after exposure to 10.5 mM of (3,3,3-trifluoropropyl)trimethoxysilane for 18 hours. The regions of interest for this trial were F 1s, O 1s, C 1s, Cl 2p3, Zr 3d5, and Si 2p3, ascribed with the same colors as Fig. 4.3. The lack of features in Cl $2p_{3/2}$ is expected as there is no chlorine present in the silane. Most notably, the F 1s region has no magnification and two peaks, not attributable to charging in the sample as no other region presents the same feature. With a total peak-area 12× larger than the F 1s in Fig. 4.2B, and less exposure time than Fig. 4.2, it is likely there is a reasoning. The F:Zr peak-area ratio is ~1.5:1 which is much higher than both the overlayer model in §3.1.2 and Fig. 4.2B. A much higher ratio of F:Zr may be attributed to two features: multilayer coverage or higher packing of the monolayer. For the overlayer model, we assumed that ~2 silanes could attach per UiO–66 face that well described the results with the organotrichlorosilane treated under rigorously water-free conditions. However the significantly larger F:Zr peak-area ratios in Fig. 4.3 as compared to Fig. 4.2 reflects the surface adsorption of a larger number of silanes when utilizing a larger concentration of a organotrialkoxysilane in the presence of catalyzing water and acetic acid, and further poses the idea that more silane may be able to attach to one face.

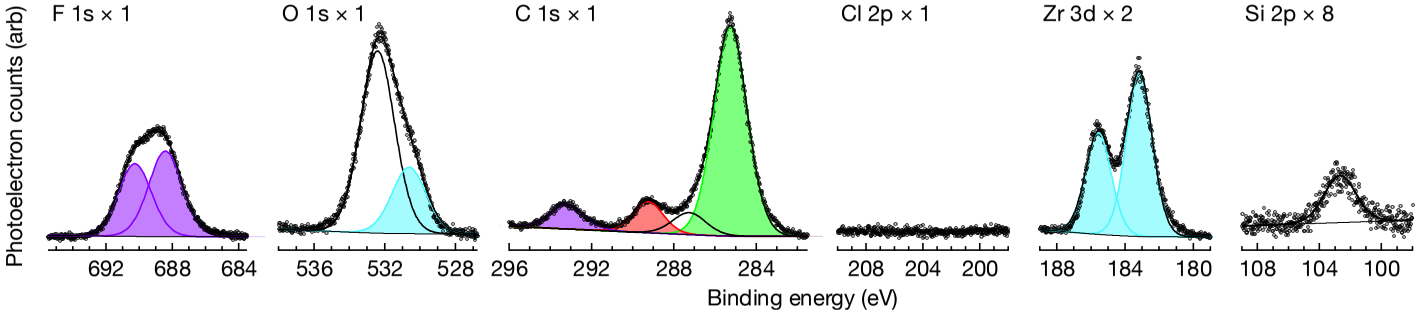

Figure 4.3: Representative XP spectra of UiO–66 after ~18 hr exposure to 10.5 mM (3,3,3-trifluoropropyl)triethoxysilane with 1 mL 0.1% acetic acid. Note the dissimilar ×1 scaling of the F 1s region as compared to the ×8 scaling in Fig. 4.2. Figure C.4 contains the full survey spectrum for this figure.

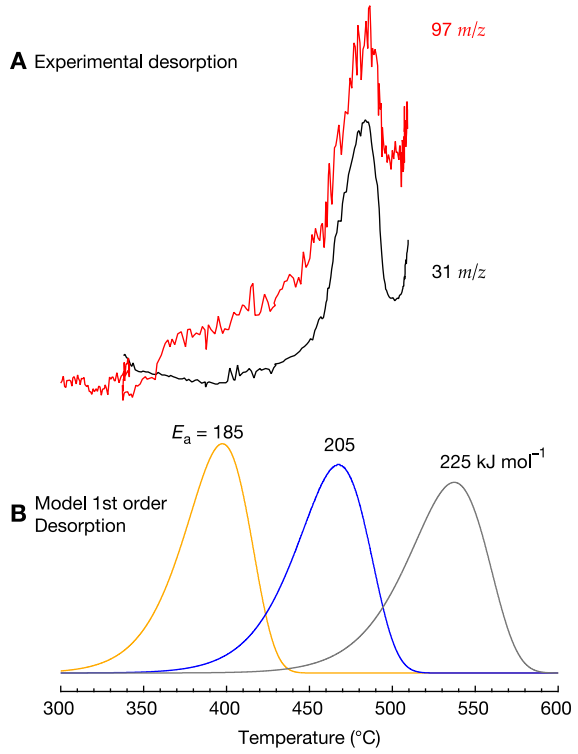

Figure 4.4: Frame A presents experimental TPD data of UiO–66 with (3,3,3-trifluoropropyl)trichlorosilane and a model of first-order desorption with $A = 1 \times 10^{13}$ s^{-1} (B).

4.3 Silane-Substrate Interaction Strength

Temperature-programed desorption was used to further probe the type and strength of the silane attachment to the surface of UiO–66. The sample was ramped up to ~520 °C while mass spectrometer data was being collected. Traces of interest were located at ~97 m/z in the red and 31 m/z in the black, representing desorption of both $(CF_3CH_2CH_2)^+$ and $(CF)^+$ respectively at ~470 °C as depicted in frame A of Fig. 4.4. Previous studies in our lab used TGA to find that total decomposition of the UiO–66 unit cell onsets around 485 °C and ramps up ~520 °C.[8] Both of the mass peaks start to upturn again after 500 °C concomitant with the onset of total UiO–66 degradation, supporting that the connectivity of the silane to the surface is done with covalent bonding almost as strong as the bonds holding the UiO–66 structure together.

CHAPTER 5

DISCUSSION

5.1 Interpretation of Theoretical and Experimental Results

The data collected supports our hypothesis of strong, covalent, monolayer-adjacent attachment of (3,3,3-trifluoropropyl)trichlorosilane to the surface of synthesized UiO–66 crystals. As mentioned, our coverage is 10× lower than coverages of similarly sized silanes,[28,29] but is a reasonable starting point with a theoretical intensity ratio of F:Zr of 0.22. Experimentally, the peak-area ratio of F:Zr from Fig. 4.2B is 0.19, which supports a monolayer-adjacent coverage. Being even less than our predicted two silanes per UiO–66 face model in Fig. 3.1A, the coverage is possibly closer to one silane per face however, the model in Fig. 3.1A is still a good representation for these results. As the TPD data suggests, there is a strong interaction between the silane and the MOF surface. Having far more than a monolayer of attachment may not have revealed this fact through TPD. The 97 *m/z* desorption trace is the assumed to be the desorption of the $(CF_3CH_2CH_2)^+$ organic fragment, implying degradation of the silicon to some degree at ~470 °C supported by work done by both Gamble[43] and Gun'ko.[44] Assuming $A = 1{\times}10^{13}\ s^{-1}$ for a first order desorption,

a decomposition of silicon would be represented by the model and an E_a of 205 ± 10 kJ mol^{-1}. Given the sub-monolayer coverage shown in Fig. 4.2B, it is likely that with a slightly higher fluorine signal and thus a greater coverage could provide more intense TPD traces.

5.2 Miscellany

The overlayer model employed in this study is a starting point for understanding the silane–UiO–66 interface. The overlayer model does not accurately represent the coverage of UiO–66 with (3,3,3-trifluoropropyl)trimethoxysilane. Depicted in Fig. 4.3, the XP spectra shows a peak-area ratio of F:Zr of 1.57, which is ~7× larger than the model. Although it is likely due to bad reagent, the faster reaction time for a less reactive silane resulting 12× more silane coverage says a lot about what is left unknown about the nature of silane attachment to UiO–66. Unlike the trichlorosilane, the trimethoxysilane required a small amount of acetic acid to kick start the reaction. It is possible that the catalyst for the reaction may have affected how the silane goes down on the surface, allowing for a higher packing density in a shorter exposure time. With the guidance of the acetic acid catalyst, the surface of UiO–66 may have become more reactive towards the silane allowing for more silanes per cluster and a more efficient coverage.

CHAPTER 6

CONCLUSIONS AND FUTURE WORK

We developed a strategy for strong covalent monolayer attachment to the surface of UiO–66 using fluorinated organosilanes. This knowledge can be applied to future research on capping and trapping with the UiO family within our group. Understanding how the capping molecules interact with the MOF on a surface level is crucial for having control of trap and release for therapeutic drug delivery. Synthesized UiO–66 crystals were exposed to fluorinated organosilanes and used in a series of experiments to probe the reactivity of and strength of bonding to the MOF surface for future trapping and capping. Analytical techniques including pXRD, XPS, Ar^+ sputtering, and TPD were used to evaluate the effectiveness of the given experiments, while we employed models of substrate overlayers and thermal desorption to further understand the results. In showing that a monolayer of silanes will covalently attach to the surface of UiO–66, we furthered our knowledge about the reactivity of the UiO family.

Going forward, there are quite a few areas that need attention with UiO–66 and the UiO family. Not only did pXRD confirm our synthesis, but it confirmed that the UiO–66 crystals that were synthesized and left in their

reaction vessel untouched would still be viable fourteen months after synthesis. This says a lot about the stability of UiO–66 and its structure and how well it could be applied to other applications. I would suggest further tests seeing how long UiO–66 can last in that environment and possibly out in air as well. Something I did not quite have the time to touch on and would have liked to was taking pXRD and TGA of UiO–66 before and after silane exposure. Using TGA after the crystal has been silanized would tell us more about the stability of the silanes and the MOF, and pXRD would possibly show how the diffraction pattern changes with silanization. Obviously, trying to attach different silanes on the surface of UiO–66, mainly (4-chloropphenyl)trimethoxysilane and 3-aminopropyltriethoxysilane, as well as TPD of (3,3,3-trifluoropropyl)trimethoxysilane to revisit the idea of silanes packing on the surface of UiO–66. Together, these ideas will further our knowledge on the stability and reactivity of the UiO family.

CHAPTER 7

REFERENCES

[1] Li, S.; Huo, F. Metal–organic framework composites: from fundamentals to applications. *Nanoscale* **2015**, *7* (17), 7482-7501. 10.1039/C5NR00518C

[2] Furukawa, H.; Cordova, K. E.; O'Keeffe, M.; Yaghi, O. M. The Chemistry and Applications of Metal-Organic Frameworks. *Science* **2013**, *341* (6149), 1230444. 10.1126/science.1230444

[3] Yang, J.; Wang, H.; Liu, J.; Ding, M.; Xie, X.; Yang, X.; Peng, Y.; Zhou, S.; Ouyang, R.; Miao, Y. Recent advances in nanosized metal organic frameworks for drug delivery and tumor therapy. *RSC Advances* **2021**, *11* (6), 3241–3263, 10.1039/D0RA09878G

[4] Yan, J.; Homan, R. A.; Boucher, C.; Basa, P. N.; Fossum, K. J.; Grimm, R. L.; MacDonald, J. C.; Burdette, S. C. On-demand guest release from MOF-5 sealed with nitrophenylacetic acid photocapping groups. *Photochemical & Photobiological Sciences* **2019**, *18* (12), 2849–2853. 10.1039/C9PP00392D

[5] Homan, R. A.; Hendricks, D. S.; Rayder, T. M.; Thein, U. S.; Fossum, K. J.; Claudio Vázquez, A. P.; Yan, J.; Grimm, R. L.; Burdette, S. C.;

MacDonald, J. C. A Strategy for Trapping Molecular Guests in MOF-5 Utilizing Surface-Capping Groups. *Crystal Growth & Design* **2019**, *19* (11), 6331–6338. 10.1021/acs.cgd.9b00818

[6] Marreiros, J.; Caratelli, C.; Hajek, J.; Krajnc, A.; Fleury, G.; Bueken, B.; De Vos, D. E.; Mali, G.; Roeffaers, M. B. J.; Van Speybroeck, V.; et al. Active Role of Methanol in Post-Synthetic Linker Exchange in the Metal–Organic Framework UiO–66. *Chemistry of Materials* **2019**, *31* (4), 1359–1369. 10.1021/acs.chemmater.8b04734

[7] Kandiah, M.; Nilsen, M. H.; Usseglio, S.; Jakobsen, S.; Olsbye, U.; Tilset, M.; Larabi, C.; Quadrelli, E. A.; Bonino, F.; Lillerud, K. P. Synthesis and Stability of Tagged UiO–66 Zr-MOFs. *Chemistry of Materials* **2010**, *22* (24), 6632–6640. 10.1021/cm102601v

[8] Dawley, R. A. Elucidating Surface Sites and Reactivity of a Zirconium-Based MOF Towards Future Capping and Trapping of Guest Molecules; Worcester Polytechnic Institute, **2021**. URL

[9] Boissonnault, J. A.; Wong-Foy, A. G.; Matzger, A. J. Core–Shell Structures Arise Naturally During Ligand Exchange in Metal–Organic Frameworks. *Journal of the American Chemical Society* **2017**, *139* (42), 14841–14844. 10.1021/jacs.7b08349

[10] Trickett, C. A.; Gagnon, K. J.; Lee, S.; Gándara, F.; Bürgi, H.-B.; Yaghi, O. M. Definitive Molecular Level Characterization of Defects in UiO–66 Crystals. *Angewandte Chemie International Edition* **2015**, *54* (38), 11162–11167. 10.1002/anie.201505461

[11] Glass, N. R.; Tjeung, R.; Chan, P.; Yeo, L. Y.; Friend, J. R. Organosilane deposition for microfluidic applications. *Biomicrofluidics* **2011**, *5* (3), 36501–365017. 10.1063/1.3625605

[12] Waddell, T. G.; Leyden, D. E.; DeBello, M. T. The nature of organosilane to silica-surface bonding. *Journal of the American Chemical Society* **1981**, *103* (18), 5303–5307. 10.1021/ja00408a005

[13] Carl, A. D.; Kalan, R. E.; Obayemi, J. D.; Zebaze Kana, M. G.; Soboyejo, W. O.; Grimm, R. L. Synthesis and Characterization of Alkylamine-Functionalized Si(111) for Perovskite Adhesion With Minimal Interfacial Oxidation or Electronic Defects. *ACS Applied Materials & Interfaces* **2017**, *9* (39), 34377-i34388. 10.1021/acsami.7b07117

[14] Moulder, J. F. S., W. F.; Sobol, P. E.; Bomben, K. D. Handbook of X-ray Photoelectron Spectroscopy; Perkin-Elmer Corporation: Physical Electronics Division, **1992**.

[15] Fairley, N. Peak Fitting in XPS. (accessed Feb. 2023).

[16] Jansson, C.; Hansen, H. S.; Yubero, F.; Tougaard, S. Accuracy of the Tougaard method for quantitative surface analysis. Comparison of the Universal and REELS inelastic cross sections. *Journal of Electron Spectroscopy and Related Phenomena* **1992**, *60* (4), 301–319. 10.1016/0368-2048(92)80025-4

[17] Shirley, D. A. High-Resolution X-Ray Photoemission Spectrum of the Valence Bands of Gold. *Physical Review B* **1972**, *5* (12), 4709–4714. 10.1103/PhysRevB.5.4709

[18] Tougaard, S. Formalism for quantitative surface analysis by electron spectroscopy. *Journal of Vacuum Science & Technology A: Vacuum, Surfaces, and Films* **1990**, *8* (3), 2197–2203. 10.1116/1.577037

[19] Gao, W.; Zielinski, K.; Drury, B. N.; Carl, A. D.; Grimm, R. L. Elucidation of Chemical Species and Reactivity at Methylammonium Lead Iodide and Cesium Tin Bromide Perovskite Surfaces via Orthogonal Reaction Chemistry. *Journal of Physical Chemistry C* **2018**, *122* (31), 17882–17894. 10.1021/acs.jpcc.8b05352

[20] Carl, A. D. Soft, Organic, Carrier-Selective Contacts at Inorganic Semiconductor Interfaces Enabled by Low-Defect Covalent Bonding. Worcester Polytechnic Institute, 2020. URL

[21] Carl, A. D.; Grimm, R. L. Covalent Attachment and Characterization of Perylene Monolayers on Si(111) and TiO_2 for Electron-Selective Carrier Transport. *Langmuir* **2019**, *35*, 9352–9363. 10.1021/acs.langmuir.9b00739

[22] Yan, J.; Carl, A. D.; Maag, A. R.; MacDonald, J. C.; Müller, P.; Grimm, R. L.; Burdette, S. C. Detection of adsorbates on emissive MOF surfaces with X-ray photoelectron spectroscopy. *Dalton Transactions* **2019**, *48* (14), 4520–4529. 10.1039/C8DT04404J

[23] Seah, M. P. Quantification of AES and XPS. In Practical Surface Analysis, 2nd ed.; Briggs, D. S., M. P. Ed.; John Wiley & Sons, 1990; pp 201-255.

[24] Ebel, M. F. Zur bestimmung der reduzierten dicke D/λ dünner Schichten mittels XPS. *Journal of Electron Spectroscopy and Related Phenomena* **1978**, *14* (4), 287–322. https://doi.org/10.1016/0368-2048(78)80005-X

[25] Fadley, C. S. Solid state—and surface—analysis by means of angular-dependent X-ray photoelectron spectroscopy. *Progress in Solid State Chemistry* **1976**, *11*, 265–343. 10.1016/0079-6786(76)90013-3

[26] Fadley, C. S. Basic Concepts of X-ray Photoelectron Spectroscopy. In *Electron Spectroscopy: Theory, Techniques and Applications*, Academic Press, 1978.

[27] Sturzenegger, M.; Prokopuk, N.; Kenyon, C. N.; Royea, W. J.; Lewis, N. S. Reactions of Etched, Single Crystal (111)B-Oriented InP To Produce

Functionalized Surfaces with Low Electrical Defect Densities. *Journal of Physical Chemistry B* **1999**, *103* (49), 10838–10849. 10.1021/jp992290f

[28] Moon, J. H.; Kim, J. H.; Kim, K.-j.; Kang, T.-H.; Kim, B.; Kim, C.-H.; Hahn, J. H.; Park, J. W. Absolute Surface Density of the Amine Group of the Aminosilylated Thin Layers: Ultraviolet-Visible Spectroscopy, Second Harmonic Generation, and Synchrotron-Radiation Photoelectron Spectroscopy Study. *Langmuir* **1997**, *13* (16), 4305–4310. 10.1021/la9705118

[29] Sugimura, H.; Moriguchi, T.; Kanda, M.; Sonobayashi, Y.; Nishimura, H. M.; Ichii, T.; Murase, K.; Kazama, S. Molecular packing density of a self-assembled monolayer formed from N-(2-aminoethyl)-3-aminopropyltriethoxysilane by a vapor phase process. *Chemical Communications* **2011**, *47* (31), 8841–8843, 10.1039/C1CC12541A

[30] Jablonski, A.; Powell, C. J. The electron attenuation length revisited. *Surface Science Reports* **2002**, *47* (2), 33-91. 10.1016/S0167-5729(02)00031-6

[31] Jablonski, A.; Powell, C. J. Effective attenuation lengths for quantitative determination of surface composition by Auger-electron spectroscopy and X-ray photoelectron spectroscopy. *Journal of Electron Spectroscopy and Related Phenomena* **2017**, *281*, 1–2. 10.1016/j.elspec.2017.04.008

[32] Seah, M. P. Simple universal curve for the energy-dependent electron attenuation length for all materials. *Surface and Interface Analysis* **2012**, *44* (10), 1353–1359. 10.1002/sia.5033

[33] Cumpson, P. J.; Seah, M. P. Elastic Scattering Corrections in AES and XPS. II. Estimating Attenuation Lengths and Conditions Required for their Valid Use in Overlayer/Substrate Experiments. *Surface and Interface Analysis* **1997**, *25* (6), 430–446. 10.1002/(SICI)1096-9918(199706)25:6<430::AID-SIA254>3.0.CO;2-7

[34] Wagner, C. D. Sensitivity Factors for XPS Analysis of Surface Atoms. *Journal of Electron Spectroscopy and Related Phenomena* **1983**, *32*, 99–102. 10.1016/0368-2048(83)85087-7

[35] Gray, H. B. Chemical Bonds: An Introduction to Atomic and Molecular Structure; University Science Books, 1994.

[36] Ferraria, A. M.; Lopes da Silva, J. D.; Botelho do Rego, A. M. XPS studies of directly fluorinated HDPE: problems and solutions. *Polymer* **2003**, *44* (23), 7241–7249. 10.1016/j.polymer.2003.08.038

[37] Blumm, J.; Lindemann, A.; Meyer, M.; Strasser, C. Characterization of PTFE Using Advanced Thermal Analysis Techniques. *International Journal of Thermophysics* **2010**, *31* (10), 1919–1927. 10.1007/s10765-008-0512-z

[38] Kanagaraj, S.; Varanda, F. R.; Zhil'tsova, T. V.; Oliveira, M. S. A.; Simões, J. A. O. Mechanical properties of high density polyethylene/carbon nan-

otube composites. *Composites Science and Technology* **2007**, *67* (15), 3071–3077. 10.1016/j.compscitech.2007.04.024

[39] Redhead, P. A. Thermal desorption of gases. *Vacuum* **1962**, *12* (4), 203–211. 10.1016/0042-207X(62)90978-8

[40] Negrov, D. A.; Eremin, E. N. Structuring Peculiarities of Polytetrafluoroethylene Modified with Boron Nitride when Activated with Ultrasonic Exposure. *Procedia Engineering* **2016**, *152*, 570–575. 10.1016/j.proeng.2016.07.657

[41] Farrando-Pérez, J.; Martinez-Navarrete, G.; Gandara-Loe, J.; Reljic, S.; Garcia-Ripoll, A.; Fernandez, E.; Silvestre-Albero, J. Controlling the Adsorption and Release of Ocular Drugs in Metal-Organic Frameworks: Effect of Polar Functional Groups. *Inorganic Chemistry* **2022**, *61* (47), 18861–18872. 10.1021/acs.inorgchem.2c02539

[42] Melillo, A.; Cabrero-Antonino, M.; Navalón, S.; Álvaro, M.; Ferrer, B.; García, H. Enhancing visible-light photocatalytic activity for overall water splitting in UiO–66 by controlling metal node composition. *Applied Catalysis B: Environmental* **2020**, *278*, 119345. 10.1016/j.apcatb.2020.119345

APPENDIX A

OPERATING OVEN IN BURDETTE LAB FOR UIO–66 SYNTHESIS

For UiO–66 synthesis, the Auto-Stop Operation feature of the oven is used. If you walk up to the oven and it is displaying something such as in the image above, you start by pressing the TIMER key once. Pressing once more on TIMER will show a blinking "AstP" on the SET TEMP screen. Pressing ENTER will change MEASURED TEMP to read "SV" and SET TEMP to read the current set temperature for the oven, along with a red blinking light next to AUTO STOP. You can adjust the SET TEMP (if not at 173°) with the "ΔV" keys. Pressing ENTER will lock in the temperature set and MEASURED TEMP will now read "tim" and SET TEMP will read the current set timer. Again, you can adjust the same way as the temperature (if not at 48 hrs). Now that time and temperature are set, you can press and hold the RUN/STOP button until the AUTO STOP light flicks on and you hear a click. The oven

Figure A.1: Photo of temperature panel on the oven used for UiO–66 synthesis

will begin heating and the timer will not start until the set temperature is reached. At the end of the timer a buzzer will sound for five minutes.

APPENDIX B

MATHEMATICA OVERLAYER MODEL

In this section, the code used to calculate the theoretical intensity ratio between fluorine and zirconium as depicted in the overlayer model in Fig. 3.1.

In[104]:=
```
(* A Berube which occurred... *)

(* A Mathematica notebook for calculating surface coverage on UiO-66 surfaces.
   If used in any way, please cite the manuscript associated with this file.
  Updated 22 Mar 2023 -- adb *)
```

In[105]:=
```
Avogadro = 6.022 × 10^23;
```

In[106]:=
```
(* OmniFocus III analyzer angle vs surf normal *)
θ = π/4;
```

In[107]:=
```
(* Sensitivity factors for Phi 5600 instrument
 with OmniFocus III analyzer and mono illumination *)
SFF = 1.000; SFZr3d = 2.216;
```

In[108]:=
```
(* UiO66 dimensions from uio66.cif all units in nanometers *)
UiO66a = 2.075 ;
```

In[109]:=
```
(* Thickness of fluorine layer based on covalent F atomic radius via H.B. Gray,
ISBN 978-0935702354 *)
dF = ∛(π/6) × 2 × 0.064
```

Out[109]=
```
0.103167
```

In[110]:=
```
(* Spacers... estimate F distance in
 between the MOF and the F layer.  Importantly,
this does not include either the MOF or the F themselves!
  If we had a distance for F - UiO cluster distance,
we could subtract FThick/2 to get this number.  We ran an AM1
 calculation on a trifluoropropyl silane attached to a
 siloxane cluster to enforce normal alignment of the Si-
C in the silane to the surface... see Figure 3.2.X in ADBThesis! *)
dFtoZr = 0.698 - dF/2;
```

In[111]:=
```
(* Now let's do attenuation lengths! *)
```

In[112]:=
```
λF = 2.517; (*Attenuation approximation length of F
 from NIST database via 10.1021/acs.langmuir.6b02471 in nm *)
λF = 2.05; (* Attenuation approximation length of
 F from 10.1016/j.polymer.2003.08.038 in nm *)
```

In[114]:=
```
(* here's the stuff for Zirconium! *)
KEZr3d = 1486.6 - 180; (* Zr3d kinetic energy in eV,
instrument work function is too small to really matter here *)
```

In[115]:=
```
UiOaveZ = (24 × 40 + 128 × 8 + 192 × 6 + 112 × 1) / (24 + 128 + 192 + 112)
 (* average atomic number of the atoms in UiO-
  66.  rlgii _thinks_ that the formula for one UiO-66 unit cell is Zr32O112C160H80*)
```

Out[115]=
$$\frac{406}{57}$$

In[116]:=
```
N[406 / 57]
```

Out[116]=
```
7.12281
```

In[117]:=
```
ρUiO66 = 4737.33/1000 × 1/Avogadro × 1/(UiO66a/10^9)^3 (* If the stoichiometry really is Zr24
   O128C192H112 then it would a mass of 4737.33 g mol and we know it is
   in a volume of UiO66a^3 and we need to get into units of kg m^-3 so *)
```

Out[117]=
```
880.519
```

In[118]:=
```
UiOaveformulamass = (91.2 × 24 + 15.9994 × 128 + 12.011 × 192 + 112) / (24 + 128 + 192 + 112)
  (* Agaaaiiiiiinnnnnnn assuming that the formula is Zr24O128C192H112 *)
```

Out[118]=
```
14.5939
```

In[119]:=
```
(* Organic layer information:*)
ORGANICaveZ = (3 × 6 + 4 × 1 + 3 × 8 + 1 × 14 + 3 × 9) / (3 + 4 + 3 + 1 + 3);
(* Average atomic number of the atoms in organic layer assuming C3O3H4Si*)
ρORGANIC = 116.15/1000 × 1/Avogadro × 1/(dFtoZr/10^9)^3 ;

ρORGANIC = 1500;
(*Assuming C3O3H4Si the mass would
    be 116.15 g/mol and is in volume of FtoZrspace so...
  making up an average between 2.2 PTFE 10.1007/s10765-008-0512-
 z and .9 HDPE 10.1016/j.compscitech.2007.04.024*)
ORGANICaveformulamass = (12.01 × 3 + 4 × 1 + 3 × 16 + 28 + 19 × 3) / (3 + 4 + 3 + 1 + 3);
(* Average formula mass from Zr-
 O bonds to top carbon which makes up organic layer*)

(*Attenuation values for zirconium through the organic layer and through itself*)
```

In[123]:=
```
λZrthroughorganic =
 0.316 × 10^12 × (ORGANICaveformulamass / (ρORGANIC × Avogadro))^(1/2) × (KEZr3d / (ORGANICaveZ^0.45 × (3 + Log[KEZr3d/27])) + 4)
```

Out[123]=
```
3.23343
```

In[124]:=
$$\lambda Zrthroughself = 0.316 \times 10^{12} \times \left(\frac{UiOaveformulamass}{\rho UiO66 \times Avogadro}\right)^{1/2} \times \left(\frac{KEZr3d}{UiOaveZ^{0.45} \times \left(3 + Log\left[\frac{KEZr3d}{27}\right]\right)} + 4\right)$$

Out[124]= 4.32533

In[125]:=
```
(* F and Zr intensity equations from Ebel,
M.F. J.Electron Spectrosc.Relat.Phenom.1978,14, 287-322. *)
```

In[126]:=
$$NF = \frac{6}{dF};$$

```
(* NF is defined as the number density of the F atom in the overlayer,
depends on how many silanes can attach per pluster of Zr
 (in this case 1 silane per cluster, two clusters per UiO surface)*)
ΦF = 1;
(* The fractional coverage by the overlayer per surface substrate atom
 in this case 1 because we are assuming uniform monolayer coverage*)
```

$$FIntensity = NF \times SFF \times \Phi F \left(1 - Exp\left[\frac{-dF}{\lambda F \times Cos[\theta]}\right]\right);$$

$$NZr = \frac{24}{UiO66a};$$

```
(* NZr is defined as the number of zirconium on the
 surface of a unit cell divided by the length of one unit cell*)
```

$$ZrIntensity = NZr \times SFZr3d \times \left(Exp\left[\frac{-0.647 - 0.103}{\lambda Zrthroughorganic \times Cos[\theta]}\right]\right);$$

$$IFtoIZr = \frac{FIntensity}{ZrIntensity}$$

```
(* This is the intensity ratio of fluorine overlayer to zirconium
  substrate for an idealy covered UiO-66 with fluorinated silanes*)
```

Out[131]= 0.216395

APPENDIX C

WIDE-AREA XPS SURVEYS

This appendix includes wide-area XP surveys for the components of Fig. 4.2A–C and Fig. 4.3.

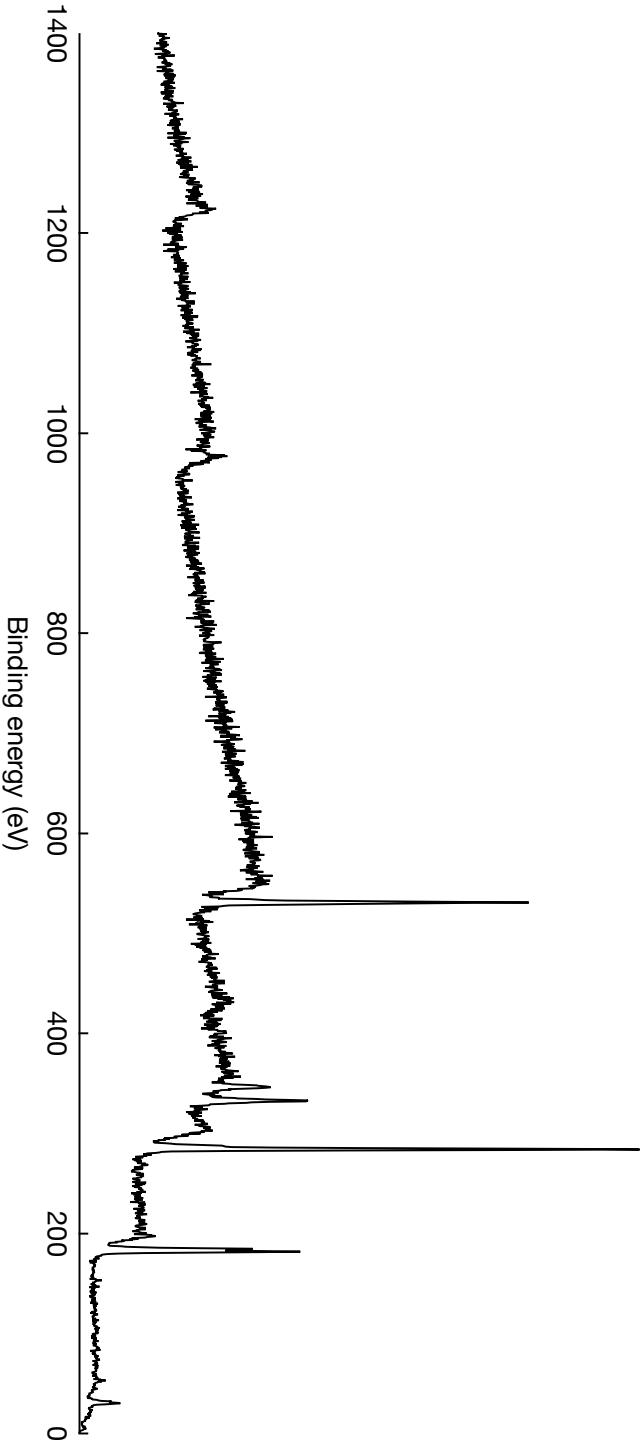

Figure C.1: Wide-area survey XP spectra for frame A of Fig. 4.2.

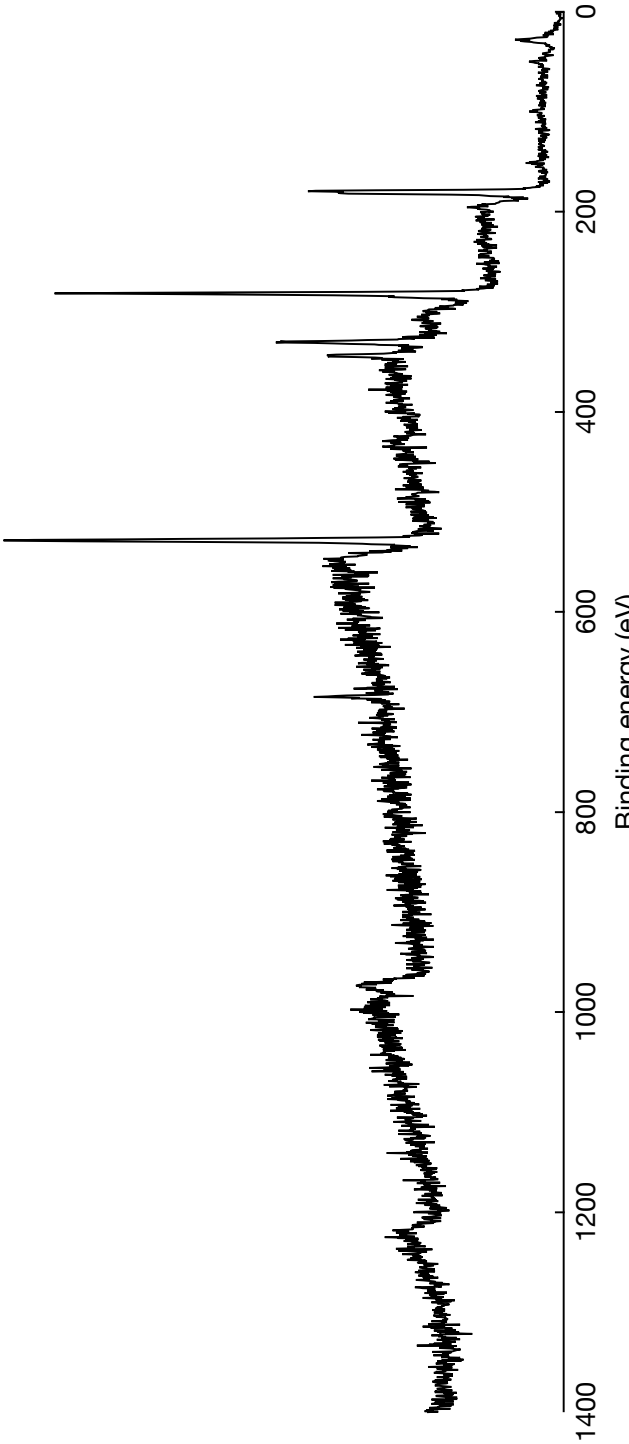

Figure C.2: Wide-area survey XP spectra for frame B of Fig. 4.2.

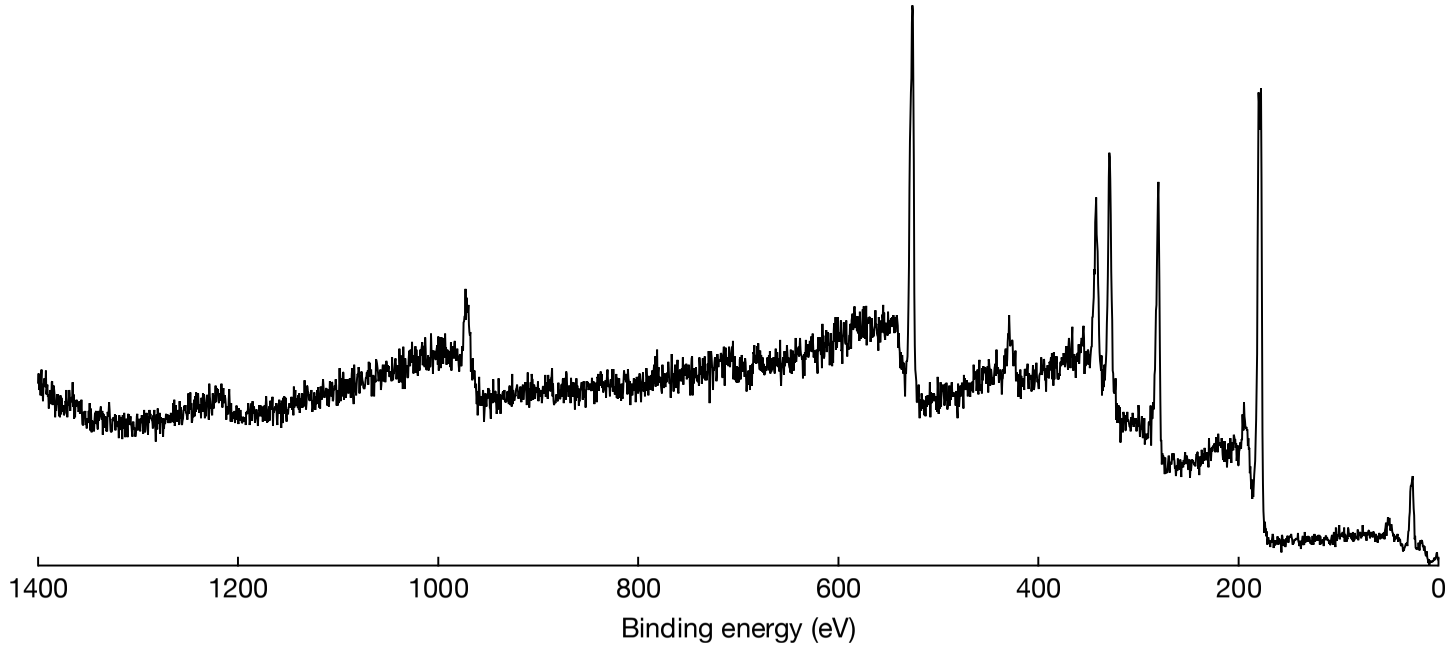

Figure C.3: Wide-area survey XP spectra for frame C of Fig. 4.2.

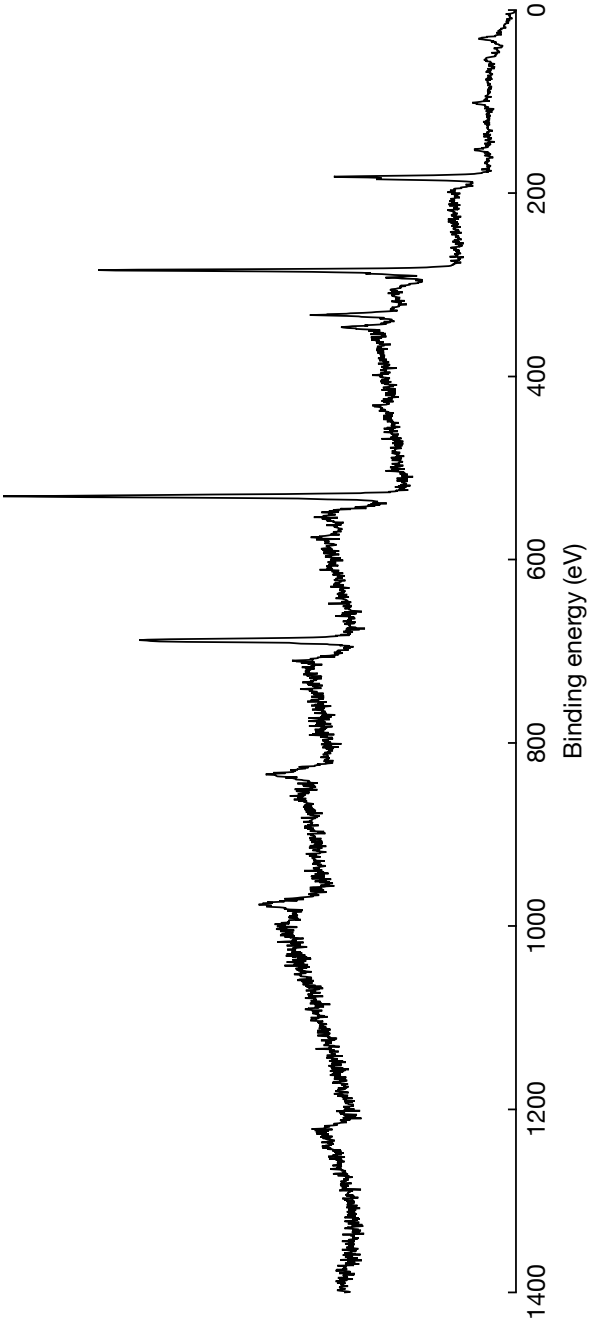

Figure C.4: Wide-area survey XP spectra for Fig. 4.3.